# Characterization of the Open Porosity of Brake Pads. II. Correlations Between Volume Porosity and Surface Area Porosity. Structural Modeling.

N. Rouge, C. Dubois and C. Vermillet

Equipe d'Accueil: Microanalyse des Matériaux U.F.R. des Sciences et Techniques 16, route de Gray F-25030 Besançon Cedex, France

### **ABSTRACT**

Mercury porosity was used for a volume quantification of the porous network of brake pads. This technique revealed three pore diameter ranges. Correlations were established between the volume porosity percentages and the surface area percentages obtained by UV/lightoptical microscopy on sections parallel and perpendicular to the brake pad friction surface. These sections showed the porosity to be structurally anisotropic, which was related to the orientations of the rigid grains. Porosity distributions were established as a function of the pore diameters computed from the surface area and aspect ratio measurements taken on sections perpendicular to the brake pad friction surface. The comparison of the computed curves and those obtained by mercury porosimetry showed that Washburn's conic model was not suitable for quantifying this porous structure, which was made up of numerous cavities connected together by constrictions. A structural model is proposed.

### 1. INTRODUCTION

In Part I, we described the development of two methods of 2-D quantification of the porosity of brake pads using image analysis techniques /1/. The method we

selected, which makes use of UV/light-optical microscopy, takes into account only part of the porosity, and does not by itself provide a complete description or volume quantification of the porous network. To fill in these 2-D information gaps, the brake pads were analyzed using mercury porosimetry which does make it possible to analyze volume parameters. Correlations established between the two types of analysis were then used for an overall characterization of the open porosity of the brake pads we studied.

### 2. THE THREE BASIC BRAKE PAD TYPES

The studies were conducted using 3 types of pads all of which were produced from the same basic A0 formula (a single initial blend of constituents, the composition of which will not be revealed). These 3 types of pads are called A0P10, A0P15 and A0P20, since their tive target porosities were 10%, 15% and 20%. Actual porosities were obtained by applying various amounts of pressure during production with all other parameters identical.

#### 3. MERCURY POROSIMETRY

## a) Experimental Technique

The equipment we used was a Coultronics 9310 porosimeter with a low pressure station for the first part of the measurements from 1 psia to 22 psia, and a high pressure station which goes from 14 psia to 30,000 psia (1 psia = 6890 Pa). A vacuum was created in the sample and mercury introduced by successive applications of increasing pressure. The penetrated volumes were measured each time the system pressure was balanced /2/. Because the structure of the porous system of the brake pads was complex /1/ and, a priori, had not been wholly characterized, Washburn's conic pore model /3/ was used systematically to link the pressure applied to the diameters of the pores. Although this model is not realistic, as this study shows, using it does nevertheless make it possible to draw up comparative variation diagrams of the cumulated volumes and the incremented volumes as a function of Washburn's diameters. Furthermore, this simple model provides a basic reference for the characterization of the porosity studied. Given the maximum pressure that can be applied to the mercury, the Washburn's diameters range between 180 µm and 6 nm, which corresponds to the ranges for capillaries, microcapillaries and mesopores defined according to the recommendations of IUPAC /4,5/.

# b) Porosimetric Study of A0P10, A0P15 and A0P20 Brake Pads

The evolution of the cumulated porosimetry curves as a function of the pore diameter was similar for all three pad types (Figure II-1). They all showed very low porosity for pore diameters of more than 10  $\mu$ m (range 1). Between 10  $\mu$ m and about 1  $\mu$ m (range 2), the higher the target porosity, the more sharply the cumulated porosity increased. Then for the small diameter pores of range 3 (less than 1  $\mu$ m), the progression of cumulated porosity was weaker, but similar for the 3 types of brake pad.

The incremented porosity curves confirmed that A0P pads were particularly differentiated for range 2. Moving from the A0P10 pads to the A0P20 pads, the peak shifted toward the larger diameter pores. What's more, the porosity rate increased over this entire range (Figure II-2). The distribution of the volume porosity percentages in the three pore diameter ranges, using Washburn's conic model, confirmed these results and showed in particular that the porosity of range 3 was practically identical for the 3 types of pads (Table II-1).

# 4. CORRELATION BETWEEN VOLUME AND SURFACE AREA POROSITY PERCENTAGES

The measurement of the surface area percentages of the 3 types of A0P pads by image analysis is described in

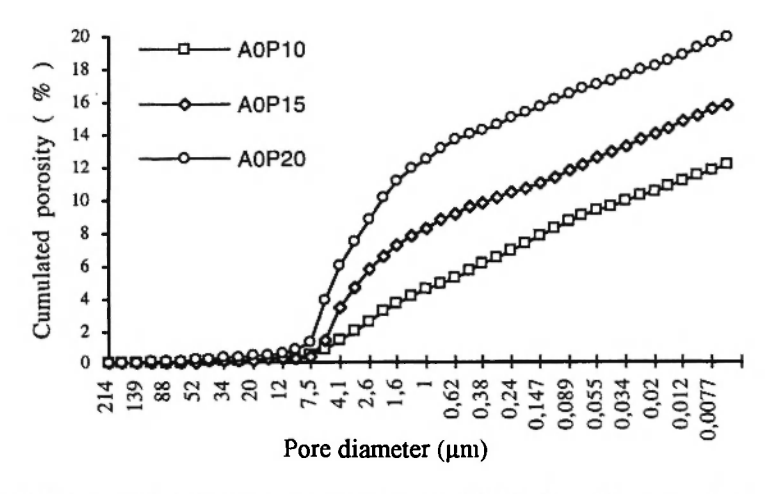


Fig. II-1: Cumulated porosity curves for the A0P10, A0P15 and A0P20 pads.

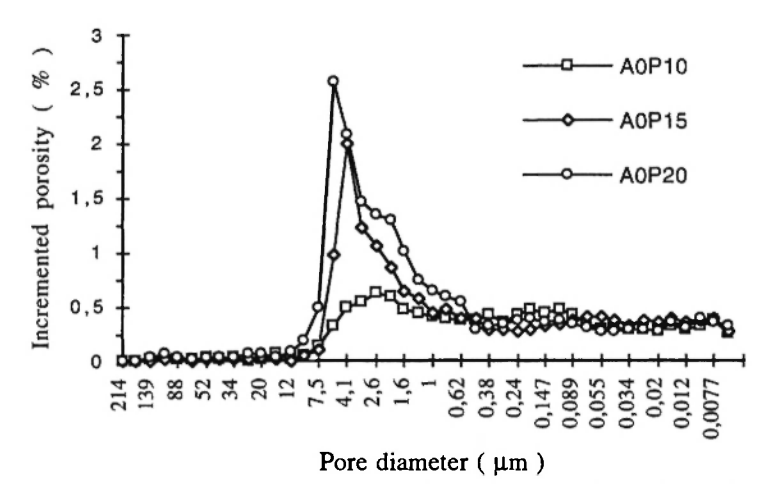


Fig. II-2: Incremented porosity curves for the A0P10, A0P15 and A0P20 pads.

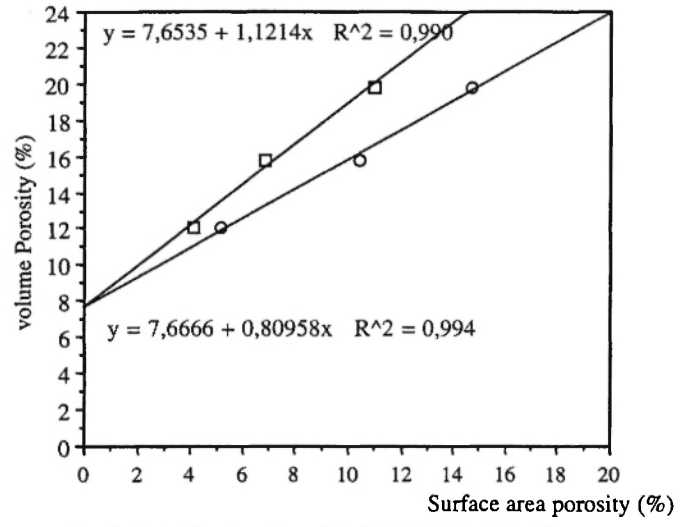
Table II-1
Volume porosity percentages as distributed in the three mercury porosimetry pore diameter ranges.

	A0P10	AOP15	A0P20
Range 1	0.4	0.3	0.8
Range 2	4.1	7.9	11.6
Range 3	7.6	7.5	7.4

Part I /1/. Volume porosity percentages as a function of the surface area percentages as measured on sections parallel and perpendicular to the pad's friction surface are shown in Figure II-3 and are linearly correlated by the following equations:

$$y = 1.12 x + 7.6$$
 for parallel sections  
 $y = 0.81 x + 7.6$  for perpendicular sections.

The ordinate for y=0 was the same for both straight lines. It corresponded to a volume porosity percentage that can be attributed to the part of the porosity that was not visible through image analysis (due to the limit of light-optical microscopy resolution). This value was very close to the porosity of the mercury porosimetry range 3. This volume percentage, practically identical for the 3 pads studied, corresponded in large part to the internal porosity of certain pad constituents and thus



- In the plane perpendicular to the pad surface.
- In the plane parallel to the pad surface.

Fig. II-3: Correlation between the volume and surface area porosity percentages.

appeared to be independent of the various amounts of pressure applied during production. This "intraconstituent" porosity was original, or created in part during production (partial decomposition of certain constituents along with degassing).

The values of the slopes of the two straight correlation lines found earlier are not equal to 1. They did not, therefore, support Delesse's claim of equality between the surface area percentage cumulated on a sufficient number of parallel sections of an object and its volume percentage /6/. Now, in this study, the surface area percentages were not measured on successive parallel planes, but on one single plane, parallel or perpendicular to the pad surface. The large number of pores analyzed was statistically sufficient, but did not allow reconstituting the volume of the pores based on the surface areas of their sections taken at random.

The difference between the surface area porosity percentages of the two sections (parallel or perpendicular to the pad friction surface) was a direct result of the structural anisotropy of the intergranular porosity, which was interconnected and oriented /1/. This anisotropy was the result of the orientations — near  $0^{\circ}$  — of the rigid, more or less oval-shaped grains.

To verify the influence of grain size on the surface area percentages, 3 pads equivalent to A0P10, A0P15 and A0P20 were made using the same overall composition and process, including the pressures, but with larger sizes of the most rigid grains (aluminum oxide, steel, brass; see Table II-2). These new pads were 210G, 215G and 222G, respectively (type G).

Differences in their incremented porosity curves, compared to those of the AOP pads, were found only in range 2 (Figure II-4). In each case, there was an increase in the peak, and thus in the intergranular

porosity. But interpreting these data in terms of Washburn's diameters was not possible given the deviation between the real structure of this porosity and that of the conic model. The intragranular nature of the constant porosity in range 3 was confirmed.

The surface area and volume porosities of these new pads were in keeping with the first two linear correlations which were recomputed for the entire set of A0P and G pads (Figure II-5). This showed that an increase in the size of the rigid grains increased the volume and surface area percentages without changing the two proportionality coefficients, which thus appeared to be numerical characteristics of the anisotropic structure of this intergranular porosity. It is important to note that the linearity between the volume and surface area percentages was recorded in a defined range of production pressures.

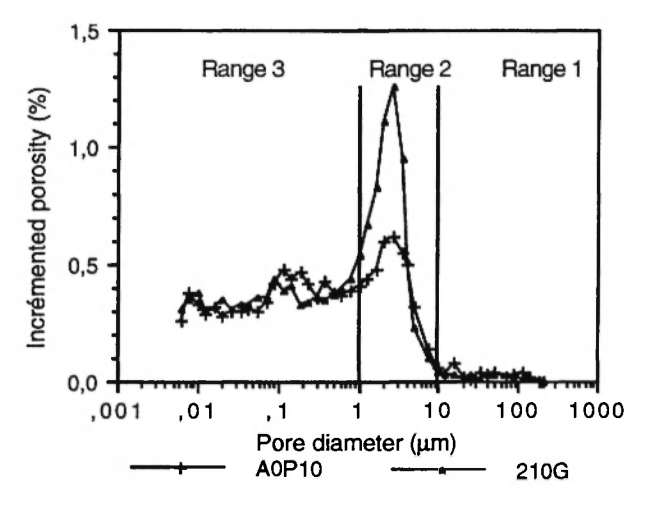
# 5. ESTIMATING THE REAL MICROPORE DIAMETERS / STRUCTURAL MODELING

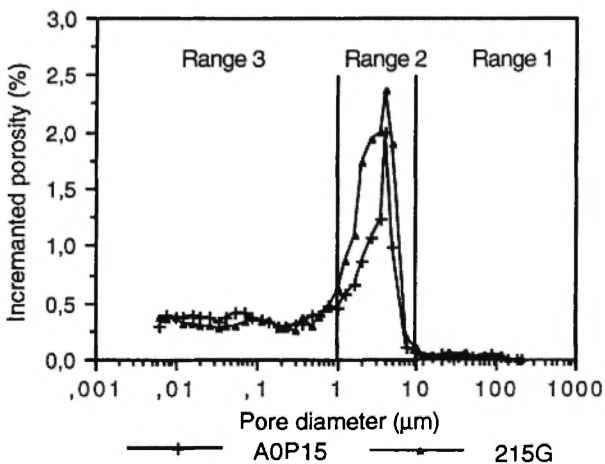
Because the computed Washburn's diameters were not suitable for graphic representation of intergranular porosity distribution, an estimate of the distribution of the real diameters was done using the 2-D analysis of the pores in the sections perpendicular to the friction surface. The binary pore images /1/ showed that this intergranular porosity was arranged as a series of surfaces which can be approximated to simple geometric shapes such as ellipses, rectangles, and, to a lesser degree, squares.

Cumulated and incremented surface area porosity curves were computed based on the pore areas and aspect ratios in order to make comparisons with the

Table II-2
Factors of increase in size of rigid grains in G pads in relation to A0P pads.

	aluminum oxide	steel	brass
Grain sizes			
by a factor of:	4-5	3	4-5





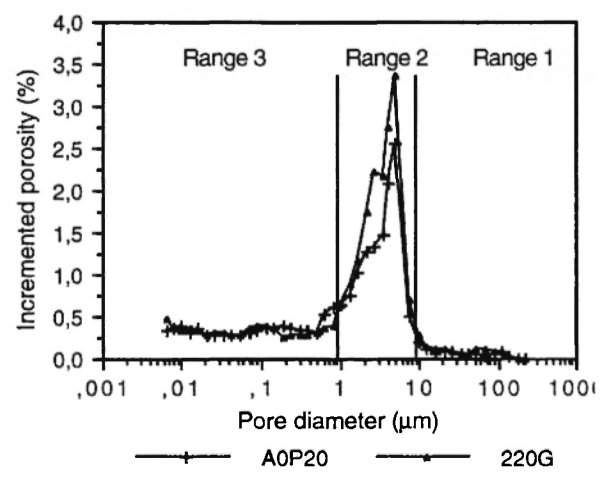


Fig. II-4: Comparison of the incremented porosity curves of the AOP and G pads.

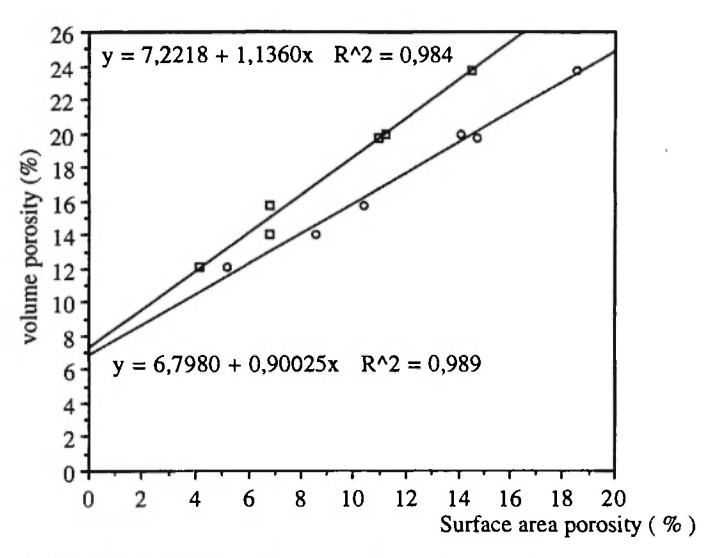


Fig. II-5: Correlations between the volume and surface area percentages of the AOP and G pads.

volume porosity percentage curves obtained from the mercury porosimetry measurements. The pore diameters were determined using the assumption that the surface areas of the pores in a section, observed at random, are cross sections of square, rectangular or elliptical pores.

Jenkins and Rao /7/ developed an equation equivalent to Washburn's for pores with elliptical cross sections: after filling an elliptical pore (short axis 2a and long axis 2b) with mercury, an equilibrium was set up between the work due to the applied pressure P and that of the contact forces (Dubinin /8/). The diameter D=2a as a function of the equilibrium pressure P and the aspect ratio  $\rho$  = a/b is given by the following relation:

$$D = [-4 \gamma \cos(\theta/P)] [(1 + \rho^2) / 2]^{1/2}$$

where

 $\gamma$  = mercury surface tension (0.48 N/m)

 $\theta$  = contact angle (140°)

In the case of a circular pore ( $\rho = 1$ ), this equation leads to Washburn's.

In comparison with Washburn's model, then, the

elliptical model introduced a factor dependent on the aspect ratio. Starting with this result, and considering the surface area and the aspect ratio measured for each pore by image analysis /1/, a diameter D was computed using the following relations which compared the pore to a square, a rectangle, or an ellipse:

$$D = \sqrt{S} (\rho = 1)$$

$$D = 2a = \left[\frac{a}{b} \cdot 2a \cdot 2b\right]^{\frac{1}{2}} = \sqrt{\rho S}$$

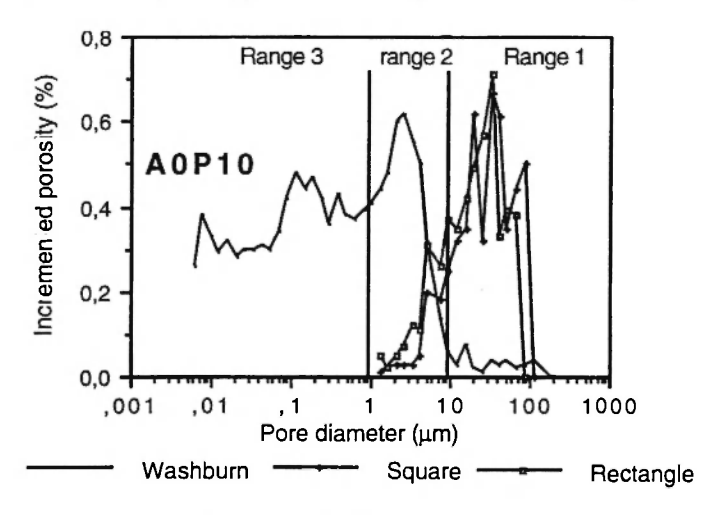
$$D = 2a = \left[\frac{4}{\pi} \cdot \frac{a}{b} \cdot \pi ab\right]^{\frac{1}{2}} = \frac{2}{\sqrt{\pi}} \sqrt{\rho S}$$

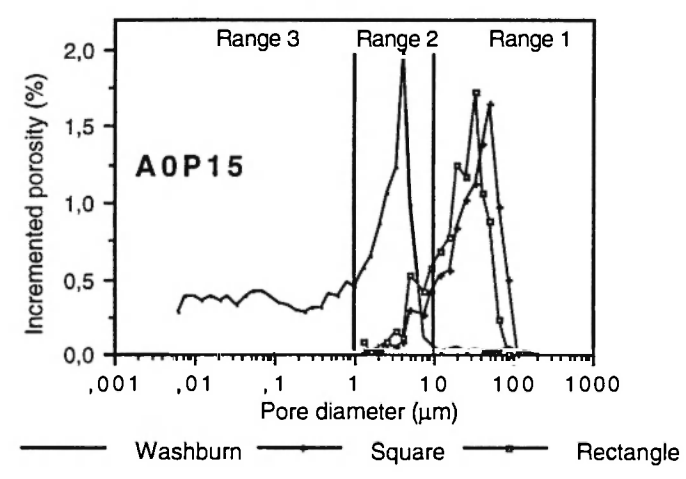
These relations make it possible to construct cumulated or incremented surface area porosity curves, by distributing the computed surface area diameters in the diameter categories obtained by mercury porosimetry. This makes the comparison of surface area and volume curves possible.

Figure II-6 shows the incremented volume porosity curves for A0P10, A0P15 and A0P20, into which the surface area curves computed from cubic and rectangular models have been transferred. The surface area porosity curves, according to both models, were relatively close to each other and similar. The curves computed with the elliptical model are not shown because they were in between the other two and very close to those of the rectangular model. The three pore models used to calculate the surface area diameters produced surface area porosity peaks whose shape and amplitude were rather similar to those from mercury porosimetry, particularly for A0P15 and A0P20.

The diameters of the intergranular pores were distributed between 200  $\mu m$  and 1.3  $\mu m$  instead of 10  $\mu m$  and 1  $\mu m$  as with mercury porosimetry; this represents an average multiplication factor of 20, the incremented surface area porosity peak being located in the mercury porosimetry range 1.

In agreement with the 2-D observations /1/, these results showed that the intergranular porosity was made up of numerous cavities joined by bottle necks (a structure like a series of interconnected "ink bottles"). Mercury porosimetry could not be used to measure the true width of these "ink bottles" since this method only takes into account their entrance diameters, going from





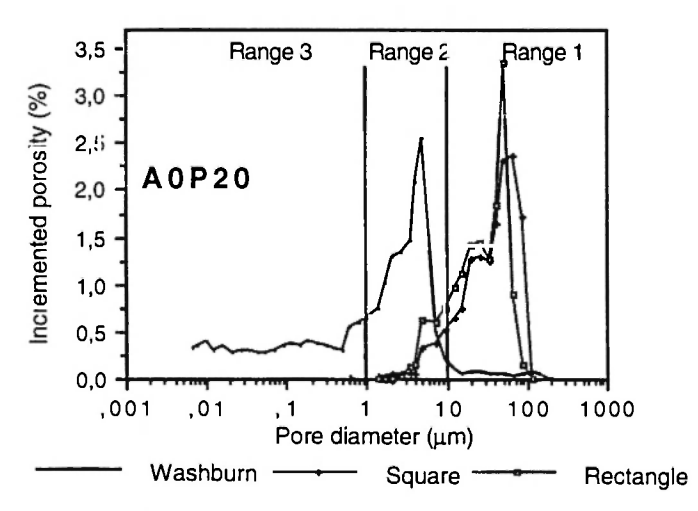


Fig. II-6: Comparison of the incremented volume porosity curves (Washburn's model) and the incremented surface area porosity curves (square and rectangular models).

the larger entrances toward the smaller ones, as a function of increasing pressure applied to the mercury.

The similarity of the two incremented curves (surface area and volume) suggested that the statistical distribution of the areas measured as a function of the computed pore diameters was linked to that of the volumes of the "ink bottles" as they were filling up. This similarity confirmed the proportional relationship between the surface area and volume percentages measured of intergranular porosity (Figure II-3), but it did not allow their coefficient of proportionality to be computed with precision.

The distribution of intergranular porosity as a function of the surface area diameters led to a more accurate representation of the true structure of this "interconnected ink bottle" porosity than that made as a function of Washburn's diameters. The complex spatial structure of the intergranular porosity cannot be compared to that of simple networks (Bethe's networks; networks of parallel or interconnected tubes with identical diameters), developed by various authors /9-11/, and does not allow 3-D geometrical modeling that can be used to quantify certain representative parameters.

#### 6. CONCLUSIONS

Image analysis and mercury porosimetry have made it possible to establish correlation between the volume and surface area percentages, correlations that characterize the structure of the brake pads studied. They showed that the intergranular porosity was structurally anisotropic, and this was linked to the orientations of the rigid grains. The comparison of the volume and surface area porosity distributions underscored the complexity of this porous structure. Moreover, it showed that Washburn's conic model was not suitable for quantifying the porosity of this composite material.

In the final analysis, brake pad porosity was divided

into two ranges:

The first range, observed by light-optical microscopy and analyzed by image analysis, was made up of intergranular porosity in the shape of "ink bottles" connected by constrictions.

The second range, with a constant porosity of about 7.5%, which corresponded to the third mercury porosimetry range, was made up of the porosity of certain constituents of the pads.

The correlation between 3D mercury porosimetry and 2D image analysis is a good means for the characterization and quantification of porous networks in materials /12/.

#### 6. REFERENCES

- N. Rouge, C. Dubois, C. Vermillet and A. Chambaudet, "Characterization of the open porosity of brake pads. I Development of 2-D porosity image analysis techniques", Sci. & Engn. Comp. Mater., accepted.
- 2. W. Douglas, Mat. Res. Symp. Proc., 137, 93 (1989).
- 3. E.W. Washburn, *Proc. Nat. Acad. Sci.*, 7, 115 (1921).
- 4. K.S.W. Sing, Pure & Appl. Chem., 57, 603 (1985).
- 5. E. Robens, TIZ International, 115, 352 (1991).
- A. Delesse, "Notice sur les travaux de Mr. A. Delesse", Gauthier-Villars, 1869; 31.
- 7. R.G. Jenkins and M.B. Rao, Powder Technology, 38, 177 (1987).
- 8. M.M. Dubinin, Chem. Rev., 60, 235 (1960).
- 9. F.A.L. Dullien, Transport in Porous Media, 6, 581 (1991).
- 10. M. Reginald, Chem. Eng. Sci., 41, 2663 (1986).
- 11. S. Reyes, Chem. Eng. Sci., 41, 333 (1986).
- C. Dubois, D. Perreux, B. Crimée, N. Rouge and J.P. Pequegnot, *Matériaux & Techniques*, in press (1995).